[Supporting Information to accompany]

High-Performing Low-Bandgap Conjugated Polymer Bearing Diethynylanthracene Units for Thin-Film Transistors

Dae Hee Lee,[a] Jicheol Shin,[a] Min Ju Cho,[a] and Dong Hoon Choi*[a]

[a]*Department of Chemistry, Research Institute for Natural Sciences, Korea University,*
5 Anam-dong, Sungbik-gu, Seoul 136-701, Republic of Korea.

* To whom correspondence should be addressed. E-mail: dhchoi8803@korea.ac.kr

1. Instrumentation: ^{1}H NMR spectra were recorded on a Varian Mercury NMR 300 MHz spectrometer using deuterated chloroform purchased from Cambridge Isotope Laboratories, Inc. Elemental analyses were performed using an EA1112 (Thermo Electron Corp.) elemental analyzer. Thermal properties were studied under a nitrogen atmosphere on a Mettler DSC 821^e instrument. Thermal gravimetric analysis (TGA) was conducted on a Mettler TGA50 (temperature rate 10 ^{o}C/min under N_2). The redox properties of the molecule were examined by using cyclic voltammetry (Model: EA161 eDAQ). Thin films were coated on a platinum plate using chloroform as a solvent. The electrolyte solution employed was 0.10 M tetrabutylammonium hexafluorophosphate (Bu_4NPF_6) in a freshly dried acetonitrile. The Ag/AgCl and Pt wire (0.5 mm in diameter) electrodes were utilized as reference and counter electrodes, respectively. The scan rate was at 50 mV/s.

Atomic force microscopy (AFM, Advanced Scanning Probe Microscope, XE-100, PSIA) operating in tapping mode with a silicon cantilever was used to characterize the surface morphologies of the thin films. The film sample was fabricated by spin-coating the chloroform solution on *n*-octyltrichlorosilane (OTS)-treated silicon wafer followed by drying at 50 ^{o}C under vacuum (solvent: chloroform, concentration of the solution: 10 mg/mL).

In order to study the absorption and emission behaviors, thin films were fabricated on quartz substrates as follows. A chloroform solution (1 wt%) was filtered through an acrodisc syringe filter (Millipore 0.45 μm, Billerica, MA, USA), which was subsequently spin-cast on quartz glass. The films were dried overnight at 60 °C for 12 h under vacuum.

Absorption spectra of the samples as films and as a solution (chloroform, concentration: 1 × 10^{-6} mole L^{-1}) were obtained using a UV–Vis spectrometer (HP 8453, photodiode array type) in the wavelength range 190–1100 nm.

Wide angle X-ray diffraction (WAXD) measurements were performed with a Rigaku D/MAX Ultimata 3. The measurements were recorded over a range of $2° < 2\theta < 45°$ and X'celerator detector operating at 40 kV and 30 mA. The film samples were fabricated by spin coating the solution on a silicon wafer followed by drying at 50°C under vacuum (solvent: chloroform, conc. of the solution: 10 mg/mL).

Grazing incidence X-ray diffraction (GI-XRD) measurements were performed at the 9A (U-SAXS) beam lines (energy = 11.260 keV, pixel size = 79.016 μm, wavelength = 1.1011 Å) at the Pohang Accelerator Laboratory (PAL). The measurements were obtained in a 2θ scanning interval between 0° and 20°; the component of the scattering vector parallel (q_{xy}) and perpendicular (q_z) to the substrate were determined as: $q = (4\pi/\lambda) \sin \theta$, where θ is half the scattering angle and λ is the wavelength of the incident radiation. The film samples were fabricated by spin-casting on OTS-SiO_2/Si, followed by drying at 50 °C under vacuum (solvent: chloroform, concentration: 10 mg/mL).

2. Synthesis

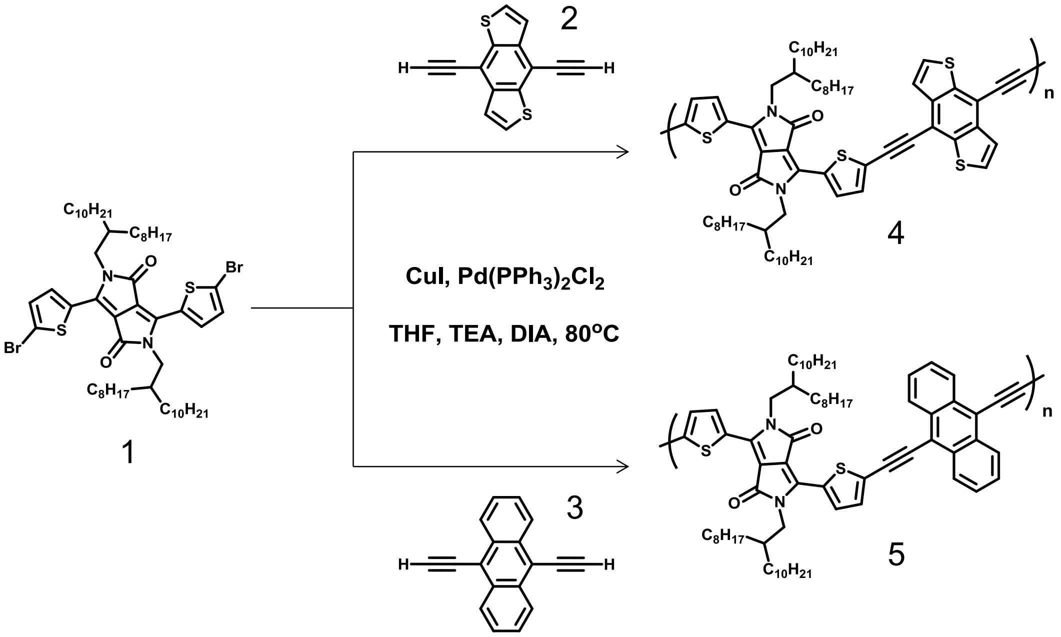

Scheme 1. Synthesis of P(DPP-BDT), **4** and P(DPP-ANT), **5**.

Materials: All chemicals were obtained from commercial sources and used without further purification. All of the reactions and manipulations were carried out under N_2 by using standard inert atmosphere and Schlenk techniques unless otherwise noted. The solvent used in inert-atmosphere reactions was dried and degassed using standard procedures. All deuterated solvents were purchased from Cambridge Isotope Laboratories, Inc

Poly[3-(5-methylthiophen-2-yl)-2,5-bis(2-octyldodecyl)-6-(5-((8-(prop-1-yn-1-yl)benzo[1,2-b:4,5-b']dithiophen-4-yl)ethynyl)thiophen-2-yl)pyrrolo[3,4-c]pyrrole-1,4(2H,5H)-dione], 4: An oven-dried, magnetic-stirred, 250-mL round-bottom flask (RBF) was charged with a solution of **1** (0.93 g, 0.91 mmol), bis(triphenylphosphine)palladium(II) dichloride (0.032 g, 0.046 mmol), and copper iodide (0.0087 g, 0.046 mmol) in a mixture of freshly distilled tetrahydrofuran (75 mL), triethylamine (15 mL), and diisopropylamine (1.5 mL). Compound **2** (0.22 g, 0.91 mmol) was then added, and the mixture was heated at 80 °C for 72 h. The dark green solution was cooled down to room temperature. The polymer was precipitated in methanol/H_2O (10:1 v/v) solution. The crude polymer was collected by filtration and then successively purified by Soxhlet extraction with acetone, hexane, and chloroform. The final product was obtained by precipitation into methanol. The product was then dried under vacuum for 1 day to get the copolymer, **4**, as a dark green solid with 89% yield (M_n = 13 552, M_w = 49 085, polydispersity (PDI) = 3.62).
^{1}H NMR ($CDCl_3$, 300MHz), δ (ppm): 8.95 (broad, 4H), 7.50 (broad, 4H), 3.92 (broad, 4H), 1.22 (broad, 63H), 0.83 (broad, 15H), Anal. Calcd. for $C_{70}H_{96}N_2O_2S_4$: C, 74.68; H, 8.60; N, 2.49; S, 11.39; found: C, 74.61; H, 8.15; N, 2.58; S, 11.63.

Poly[3-methyl-6-(5-((10-((5-methylthiophen-2-yl)ethynyl)anthracen-9-yl)ethynyl)thiophen-2-yl)-2,5-bis(2-octyldodecyl)pyrrolo[3,4-c]pyrrole-1,4(2H,5H)-dione], 5: An oven-dried, magnetic-stirred, 250-mL RBF was charged with a solution of **1** (0.56 g, 0.55 mmol), bis(triphenylphosphine)palladium(II) dichloride (0.019 g, 0.028 mmol), and copper iodide (0.0053 g, 0.028 mmol) in a mixture of freshly distilled tetrahydrofuran (45 mL), triethylamine (5 mL), and diisopropylamine (1 mL). Compound **3** (0.13 g, 0.55 mmol) was then added, and the mixture was heated at 80 °C for 72 h. The dark green solution was cooled down to room temperature. The polymer was precipitated in methanol/H_2O (10:1 v/v) solution. The crude polymer was collected by filtration and then successively purified by Soxhlet extraction with acetone, hexane, and chloroform. The final product was obtained by precipitation into methanol. Then, the product was dried under vacuum for 1 day to get the copolymer, **5**, as dark green solid with 87% yield (M_n = 25 984, M_w = 218 581, PDI = 8.41).

^{1}H NMR ($CDCl_3$, 300MHz), δ (ppm): 8.95 (broad, 4H), 8.47 (broad, 4H), 7.64 (broad, 4H), 3.92 (broad, 4H), 1.24 (broad, 63H), 0.83 (broad, 15H), Anal. Calcd. for $C_{74}H_{100}N_2O_2S_2$: C, 79.80; H, 9.05; N, 2.52; S, 5.76; found: C, 79.80; H, 8.97; N, 2.45; S, 5.75.

3. OTFT device fabrication: To characterize TFT performance, bottom-gate top-contact device geometry was employed. On the heavily n-doped SiO_2/Si substrate, the spin-coated films (thickness ~50–60 nm) of P(DPP-BDT) and P(DPP-ANT) were prepared with chloroform as a solvent. Surface modification was carried out with OTS to make hydrophobic dielectric surface. Source and drain electrodes were then thermally evaporated (100 nm) through shadow mask with channel width and length of 1500 μm and 100 μm, respectively, for TFT devices. All the devices we fabricated in this study were clearly isolated to achieve negligible gate leakage current. All the field effect mobilities were extracted in the saturation regime using the relationship $\mu_{sat} = (2I_{DS}L)/(WC(V_G - V_{th})^2)$, where I_{DS} means saturation drain current, C is capacitance of SiO_2 dielectric, V_G is gate bias, and V_{th} is threshold voltage. The device performance was evaluated in air using 4200-SCS semiconductor characterization system.

3. GPC analysis

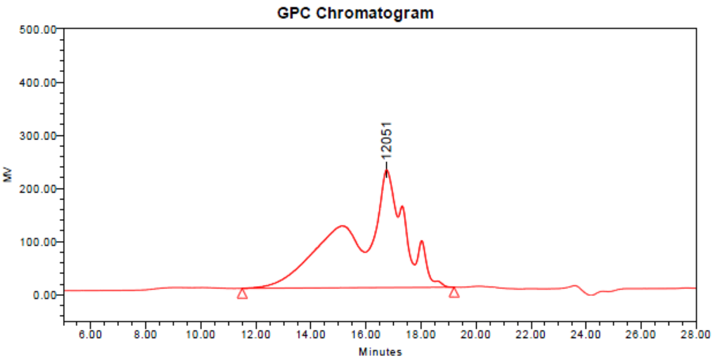

Peak Results

	Peak name	Mn	Mw	MP	Polydispersity	Mz	Mz/Mw	% Area
1	Peak1	13552	49085	12051	3.622010	157297	3.204565	100.00

Figure 1S. GPC data of P(DPP-BDT).

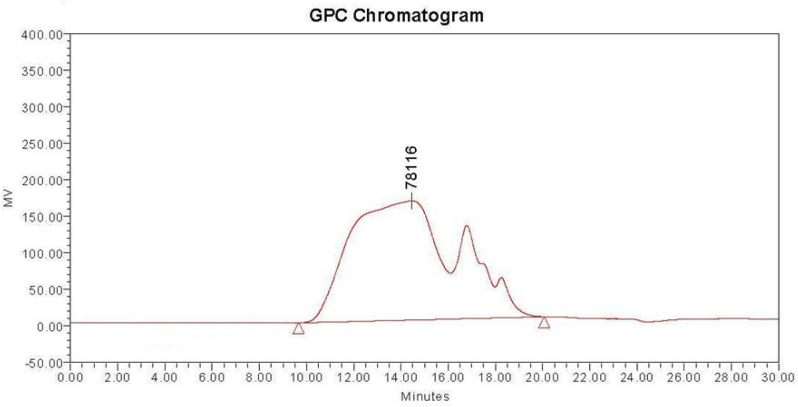

Peak Results

	Peakname	Mn	Mw	MP	Polydispersity	Mz	Mz/Mw	% Area
1	Peak1	25984	218581	78116	8.412026	611364	2.796966	100.00

Figure 2S. GPC data of P(DPP-ANT).

4. NMR spectroscopy

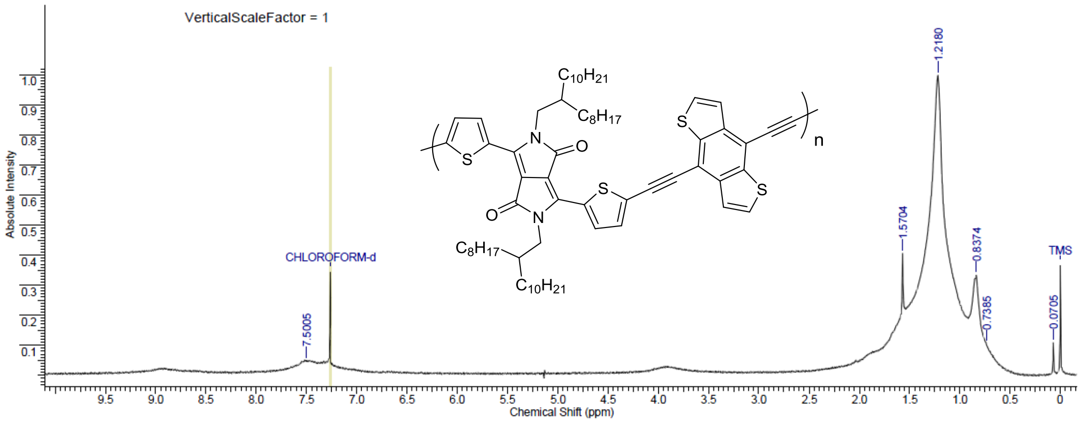

Figure 3S. NMR spectrum of P(DPP-BDT).

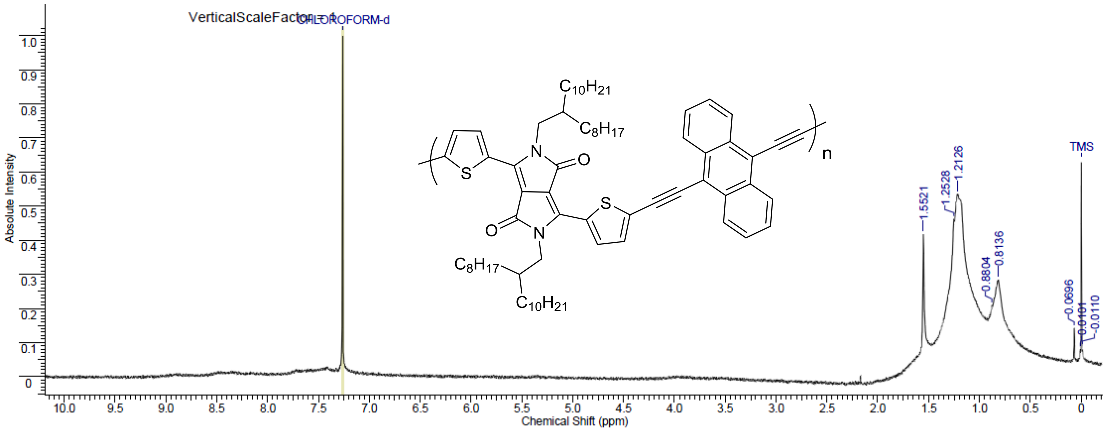

Figure 4S. NMR spectrum of P(DPP-ANT).

5. Thermal analysis

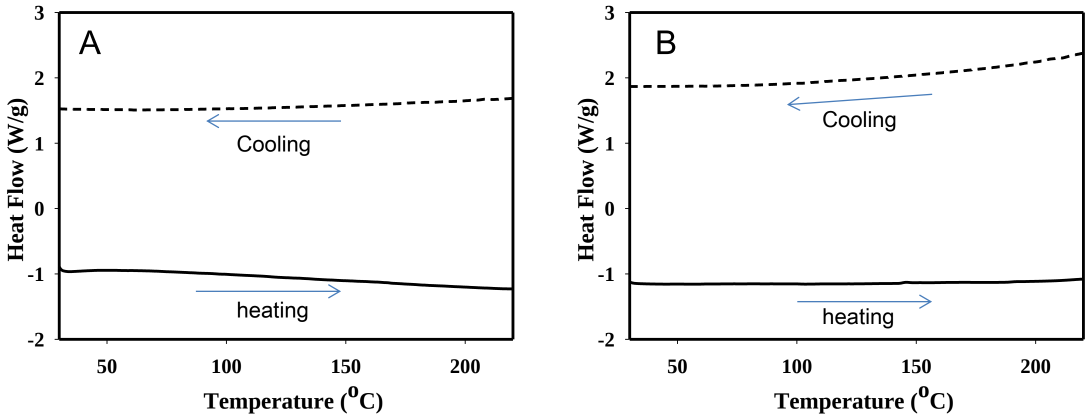

Figure 5S. DSC thermogram of (A) P(DPP-BDT) and (B) P(DPP-ANT).

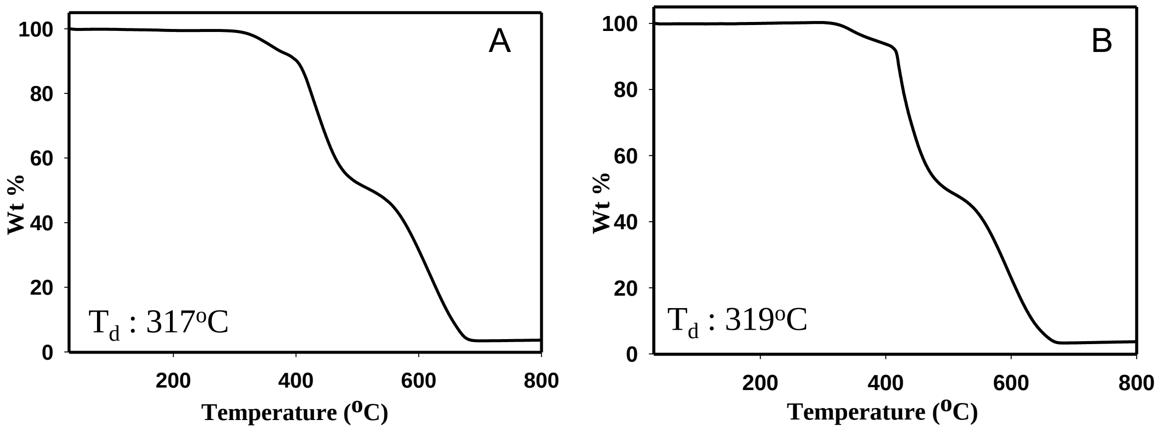

Figure 6S. TGA thermogram of (A) P(DPP-BDT) and (B) P(DPP-ANT).

Thermal decomposition temperatures of P(DPP-BDT) and P(DPP-ANT) were monitored in TGA thermograms and were found to be around 317 and 319 °C, respectively. DSC measurement was performed at a heating (cooling) scan rate of 10 (-10) °C/min under nitrogen, with the highest temperature limited to a value below the decomposition temperature. No clear transitions were observed.

6. Density functional theory calculation: To estimate the geometry and molecular energies of frontier orbitals for P(DPP-BDT) and P(DPP-ANT), density functional theory (DFT) calculations were performed using the Spartan'10 program at the B3LYP/6-31G* level. As shown in Figures 7S and 8S, the largest coefficients in the HOMO orbitals are delocalized from DPP to thiophene unit through conjugated BDT or ANT unit. They show that the planarity of the conjugated unit was sustained with a small degree of disorder, and P(DPP-BDT) and P(DPP-ANT) show small calculated bandgap energies of 2.34 and 2.13 eV, respectively.

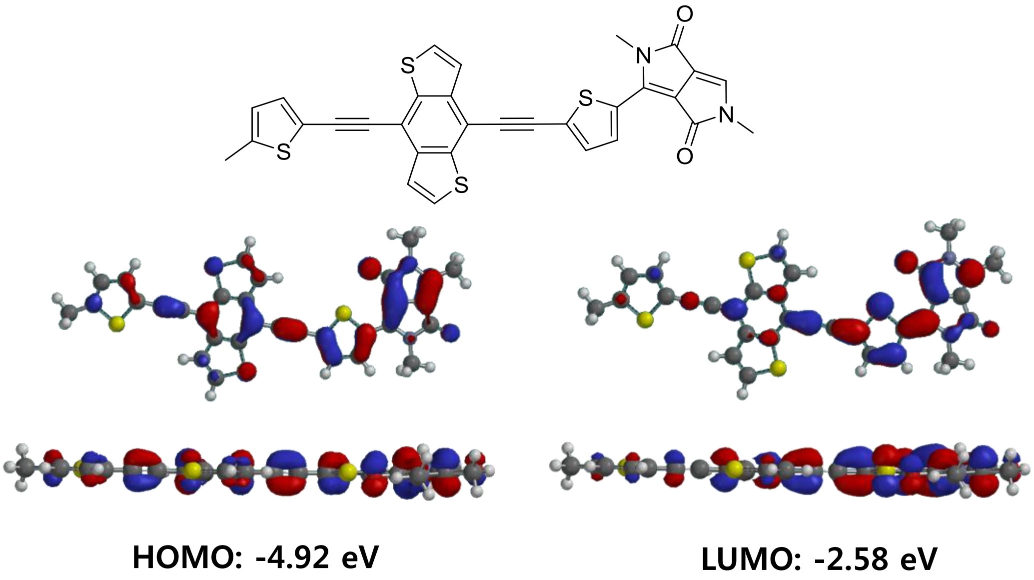

Figure 7S. HOMO/LUMO levels of P(DPP-BDT) used to calculate the theoretical molecular orbitals.

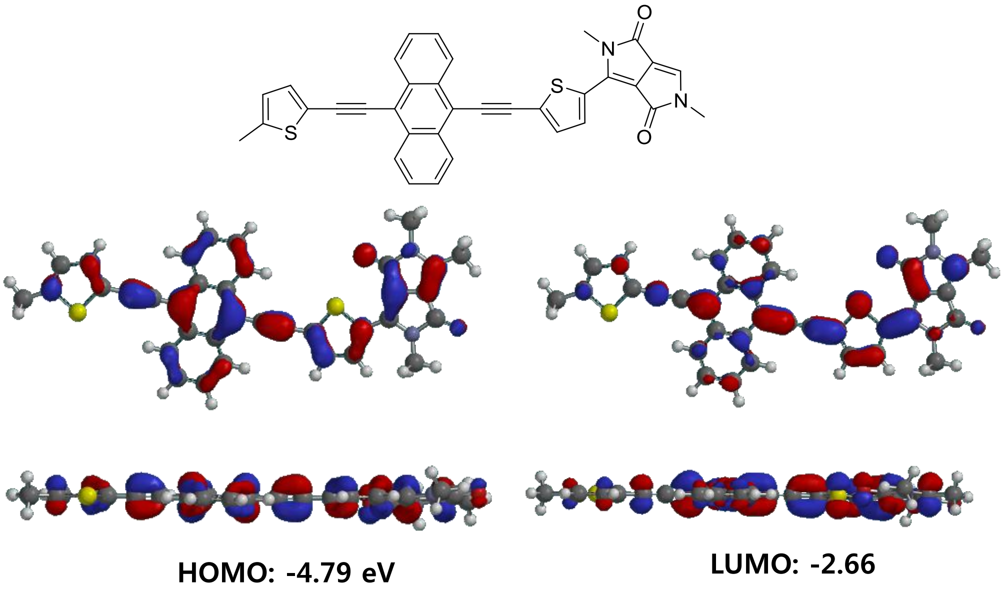

Figure 8S. HOMO/LUMO levels of P(DPP-ANT) used to calculate the theoretical molecular orbitals.

7. Wide-angle X-ray diffraction (WAXRD) analysis of P(DPP-BDT) and P(DPP-ANT)

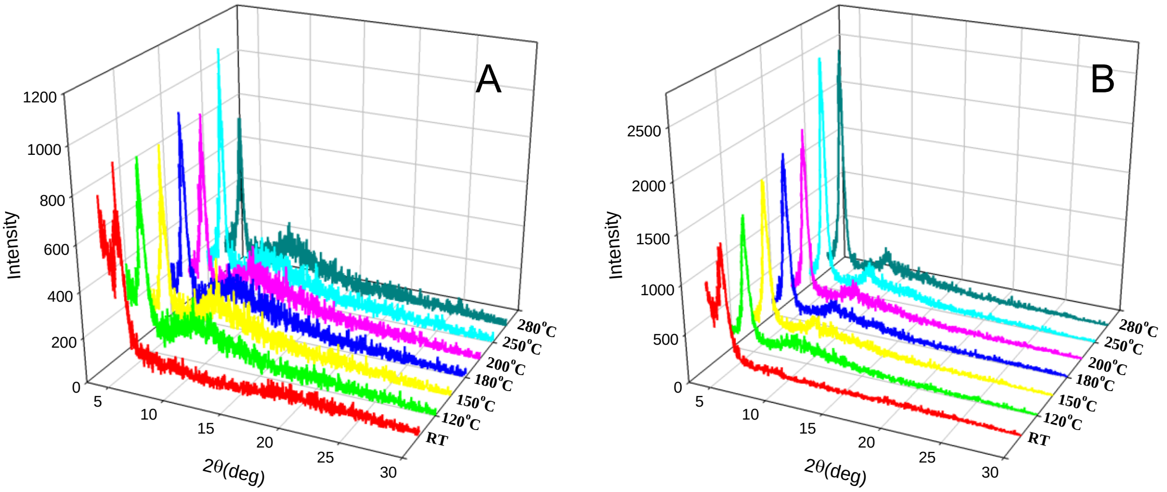

Figure 9S. XRD analysis of (A) P(DPP-BDT) and (B) P(DPP-ANT) thin films with the temperature.

8. Atomic force microscope images

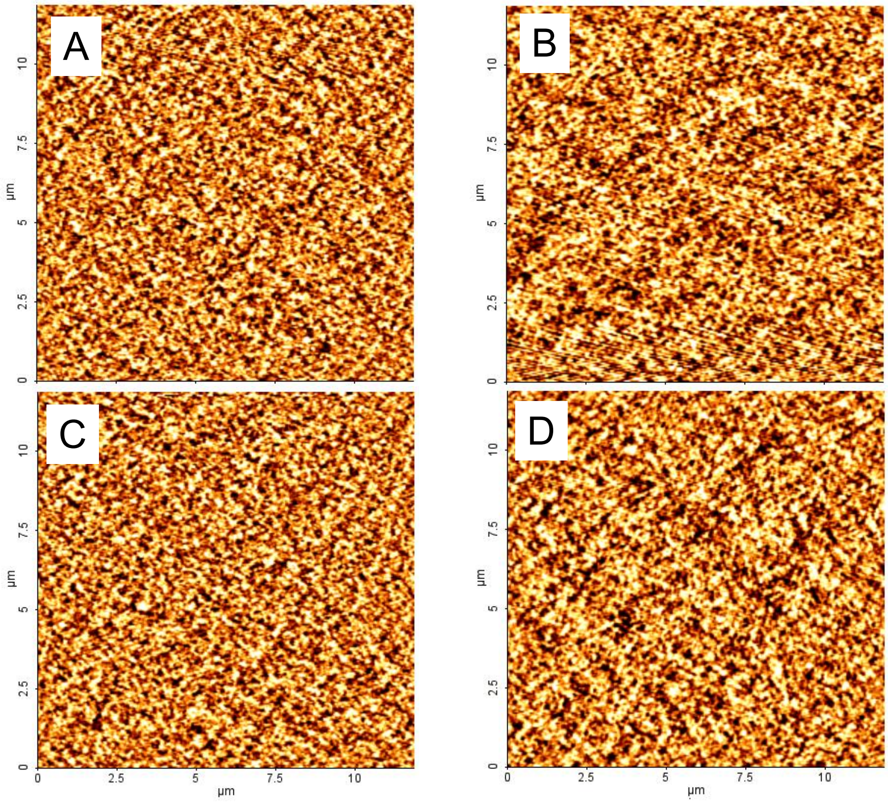

Figure 10S. Atomic force microscopy (AFM) images of the thin films of (A, C) P(DPP-BDT) and (B, D) P(DPP-ANT) thin films. (A) and (B) pristine film, (C) and (D) thermally annealed film at 250°C.

9. Device performances of TFT devices based on two polymers

Table 1S. Device properties of TFTs based on two polymers

Polymer	**SAM**	**Annealing (250°C)**	***W/L* (μm)**	**$I_{on}/_{off}$ (V)**	**V_{TH} (V)**	**μ ($cm^2V^{-1}s^{-1}$)**		
						Average	**Standard Deviation**	**Max.**
P(DPP-BDT)	OTS[a]	before	1500/100	10^6	+1.0	0.26	0.07	0.37
		After	1500/100	10^7	-1 .0	0.82	0.23	1.14
P(DPP-ANT)	OTS[a]	before	1500/100	10^6	+2.7	0.68	0.18	0.87
		After	1500/100	10^6	+3.0	1.46	0.28	1.90

[a] **Octyltrichlorosilane.**

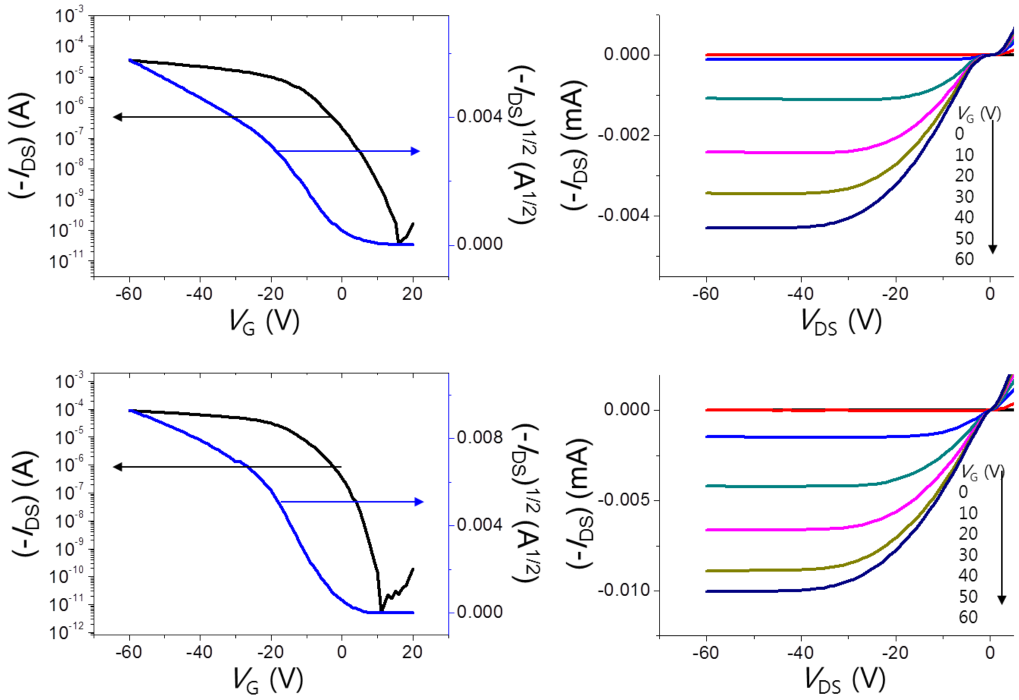

Figure 11S. Transfer (A, C) and output curves (B, D) of the TFT device fabricated with the pristine and thermally annealed P(DPP-BDT) films. (A) and (B): pristine film, (b) and (D) : thermally annealed film. *Annealing conditions: 250 °C for 10 min. *OTS-SiO_2/Si gate insulator; The device performances were measured in air.

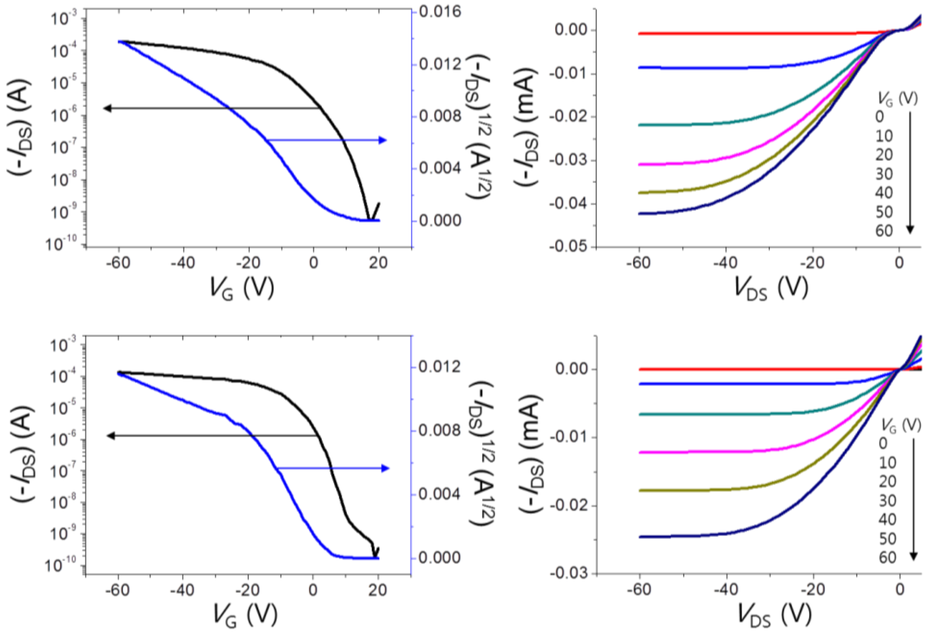

Figure 12S. Transfer (A, C) and output curves (B, D) of the TFT device fabricated with the pristine and thermally annealed P(DPP-ANT) films. (A) and (B): pristine film, (b) and (D) : thermally annealed film. *Annealing conditions: 250 ^{o}C for 10 min. *OTS-SiO_2/Si gate insulator; The device performances were measured in air.

► **Cyclic Stability of TFT devices**

1. P(DPP-BDT)-based TFT

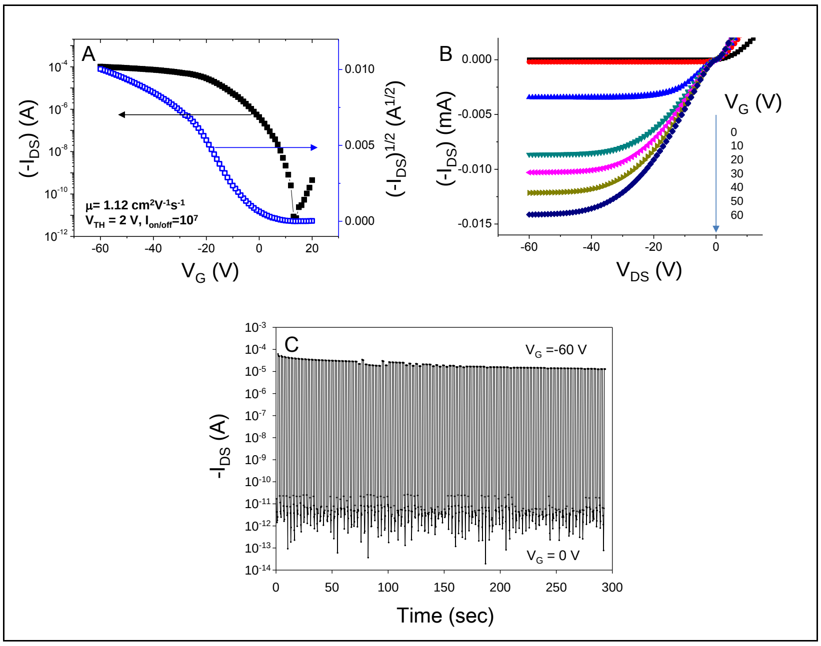

Figure 13S. (A) Transfer and (B) output curves of the TFT device fabricated with thermally annealed (250 °C for 10 min) P(DPP-BDT) film. *OTS-SiO_2/Si gate insulator; the device performances were measured in air. V_{DS} = -100 V. (C) Operational stability of the carrier mobility over 100 ON/OFF cycles.

2. P(DPP-ANT)-based TFT

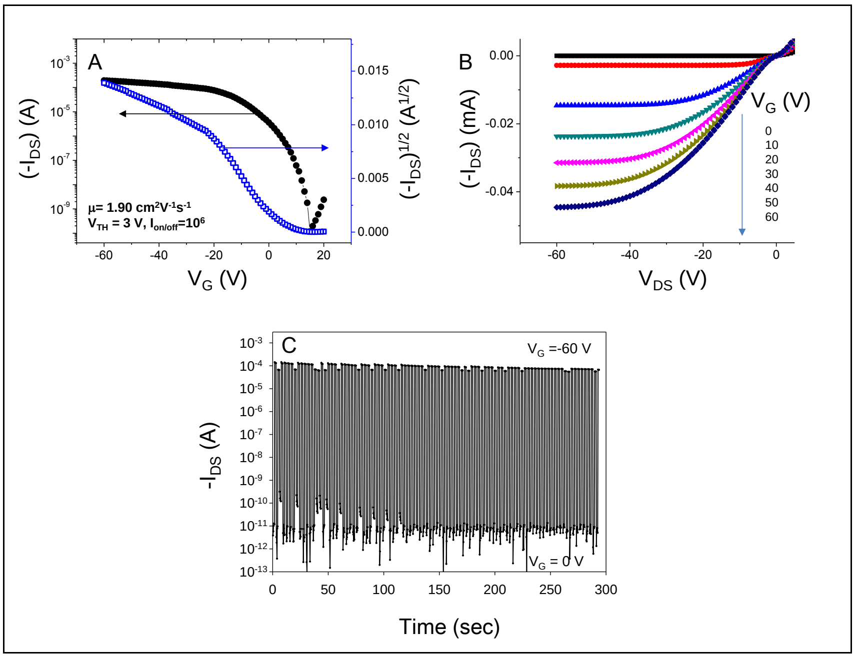

Figure 14S. (A) Transfer and (B) output curves of the TFT device fabricated with thermally annealed (250 °C for 10 min) P(DPP-ANT) film. *OTS-SiO_2/Si gate insulator; the device performances were measured in air. V_{DS} = -100 V. (C) Operational stability of the carrier mobility over 100 ON/OFF cycles.

We fabricated new TFT devices for investigating the operational stability over 100 cycles in 300 sec. The TFTs made of P(DPP-BDT) and P(DPP-ANT) also exhibited very high carrier mobilities of 1.12 and 1.90 $cm^2V^{-1}s^{-1}$, respectively. (see Figure 13S (A and B) and Figure 14S (A and B)) Under switching the gate voltage, (i.e. V_G= -60 V and 0 V), we measured the modulation of drain current (I_{DS}). In the devices made from P(DPP-BDT) and P(DPP-ANT), we observed fairly good operating cyclic stability as they showed small decrease of the current on/off ratio in ~100 cycles. The long-term stability at ambient conditions will be further investigated.